Crossover from two- to three-dimensional gold particle shapes on CaO films of different thicknesses

Xiang Shao, Niklas Nilius,* and Hans-Joachim Freund
Fritz-Haber-Institut der Max-Planck-Gesellschaft, Faradayweg 4-6, D-14195 Berlin, Germany
(Received 10 January 2012; revised manuscript received 13 March 2012; published 29 March 2012)

The growth of Au particles on Mo(001)-supported CaO films has been investigated as a function of film thickness by means of scanning tunneling microscopy and spectroscopy. Whereas, monolayer Au islands develop in the low-thickness regime [1–25 monolayers (ML)], formation of three-dimensional (3D) deposits is revealed above 40-ML film thickness. The two-dimensional (2D) growth morphology is ascribed to a charge transfer out of the CaO/Mo support into the adparticles, resulting in a reinforcement of the Au-CaO interface interaction and a strong preference for a wetting growth of gold. In the limit of ultrathin films, this charge transfer is governed by electron tunneling from the Mo substrate into the Au islands and is driven by the different Fermi levels of both systems. Although tunneling transport breaks down beyond 5–10-ML film thickness, the signature of charge-mediated Au growth remains detectable for even thicker films. This finding suggests the presence of intrinsic charge centers in the CaO film that are able to donate electrons to the gold. We relate these donor centers to Mo ions that spontaneously have diffused from the Mo support into the CaO lattice during growth. Given the low mobility of Mo in the oxide matrix, the donor concentration diminishes with film thickness and, hence, the ability of the CaO to transfer electrons into the Au deposits. Consequently, the 2D growth behavior of Au changes into the 3D regime that is characteristic for metals on inert oxide surfaces. Spectroscopic characterization of the Au particles revealed pronounced electron quantization and Coulomb charging effects due to the reduced island size.

DOI: 10.1103/PhysRevB.85.115444 PACS number(s): 68.43.Fg, 68.47.Gh, 73.40.Ns, 68.37.Ef

I. INTRODUCTION

The physical and chemical properties of metal particles are governed not only by their size, but also by the arrangement of atoms inside the aggregate, i.e., the shape.[1] This has been shown in numerous gas-phase experiments in which metal clusters of identical atom count but different shape displayed large variations in the electronic structure.[2] The pronounced shape effects have been explained by the different orbital overlaps between the particle atoms, which in turn, govern the degree of electron delocalization and band formation. Whereas, the shape dependence of the electronic structure diminishes with increasing particle size, it remains relevant when it comes to optical and chemical properties. The energy of plasmon excitations, being the dominant optical response of metal particles, sensitively depends on the shape but hardly on the size of the particles even in the 10–100-nm range.[3,4] Also, the adsorption behavior and, hence, the catalytic reactivity was found to vary with particle geometry. For identical atom counts, those particles with the highest fraction of surface atoms and the least compact geometry turned out to be the most active.[5,6] Strong shape effects also have been identified for other particle properties, such as the ionization potential and electron affinity, the heat capacity, and even the melting temperature.[1] Given this importance, immense efforts have been taken to tailor the particle shape both in the gas phase and on the solid surfaces.[7,8]

Several parameters were found to determine the equilibrium geometry of supported metal particles with the surface free energy of substrate and admetal as well as the interface adhesion being the most significant ones.[9–11] As the first two quantities are fixed once the desired material combination is selected, only the latter remains accessible for modifying the particle shape. In general, a large interface coupling favors the development of flat 2D islands, whereas, tall 3D deposits grow in the limit of small interface adhesion. The metal-support interactions can be tuned by different functionalization processes, e.g., by coating the substrate with a chemically inert spacer layer[12,13] or by generating artificial binding sites in the surface via defect formation[14] or hydroxylation.[15] Recently, the charge state of metal deposits was identified as an additional parameter that controls the metal-support interaction and, hence, the particle geometry.[16] Especially on highly ionic oxide materials, charged adsorbates experience a strong adhesion due to Coulomb interactions in combination with polaronic distortions of the substrate lattice. Negatively charged Au atoms, for example, were found to double their binding strength to MgO(001) compared to their neutral counterparts.[17] As a result, charged Au deposits preferentially adopt 2D geometries, whereas, 3D shapes prevail in the absence of excess electrons.[16,18] The charge state of a metal deposit might be altered by two approaches, which are charge transfer from suitable donor states inside the oxide lattice[19,20] or, in the case of ultrathin oxide films, electron tunneling from the metal substrate beneath.[17,18,21] The latter effect breaks down at 5–10-ML film thickness and, therefore, enables tailoring of the particle geometry only on thin-film supports.

In this paper, we have analyzed the equilibrium shape of Au particles grown on a CaO/Mo(001) thin film by means of scanning tunneling microscopy (STM). We observe a gradual crossover from 2D to 3D particle shapes when increasing the oxide thickness from 20 to 40 ML. On the basis of earlier papers[17,18,21] and spectroscopic evidence, we connect this shape evolution to charge-transfer processes from the thin-film support into the Au deposits, which diminish in thicker films. However, the critical thickness for the shape crossover was found to be larger than in other thin-film systems, suggesting that additional charge donors are present in our CaO/Mo films.

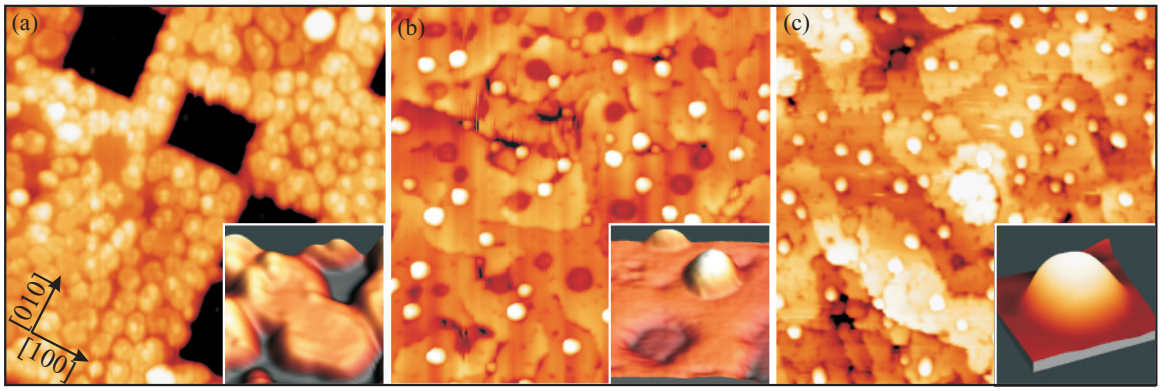

FIG. 1. (Color online) STM topographic images of (a) 20-ML-, (b) 30-ML-, and (c) 40-ML-thick CaO/Mo(001) films covered with 0.7-ML Au [100×100 nm^2, (a) -5.0 V, (b) and (c) $+6.5$ V]. The Au particle geometry evolves from 2D to 3D with increasing film thickness as visualized in the 3D representations shown in the insets (10×10 nm^2). The 2D islands in (b) and (c) appear as depressions at the actual imaging conditions

II. EXPERIMENTAL DETAILS

The CaO films were prepared by reactive Ca deposition in 5×10^{-7} mbar O_2 onto a sputtered and annealed Mo(001) surface.[22] To stimulate crystallization, the films were annealed to 1000 K in vacuum for 10 min. Quality and thickness of the films were examined with low-energy-electron diffraction (LEED) that turned out to be sensitive to the number of deposited layers. Whereas, a sharp 2×2 superstructure with respect to the Mo spots was found for thin films (1–4 ML), a square (1×1) pattern with pronounced satellites, and a plain (1×1) pattern appeared above 5- and 15-ML nominal thickness, respectively. The different diffraction patterns can be used as fingerprints for different CaO phases.[22] The (2×2) pattern is produced by a Ca-Mo mixed oxide that forms on top of the Mo(001) as a result of Mo interdiffusion. The mixed phase has a rock-salt structure with one quarter of the Ca ions being substituted by Mo. Its lattice parameter is 5% smaller than the one of bulk CaO, which reduces the lattice mismatch with the Mo(001) support. Because of the limited mobility of the Mo ions, the formation of the mixed phase terminates at around 4-ML thickness, and pure CaO(001) starts growing on top of the wetting layer. In this case, the reemerging lattice mismatch is removed by the formation of dislocation lines and mosaic structures as evidenced by the satellites around the (1×1) LEED spots.[23] Above 15-ML thickness, the individual oxide grains merge into a closed film, which exhibits an atomically flat surface and displays the sharp (1×1) LEED pattern of a fully relaxed CaO lattice.

Gold has been dosed from an e-beam evaporator onto the CaO(001) films at room temperature using typical growth rates of 0.5 ML per minute. After preparation, the samples immediately were transferred into a custom-built ultrahigh vacuum STM operated at 10 K. While surface imaging was performed in the constant current mode at 5–20 pA, the electronic properties were deduced from conductance spectra taken with a lock-in amplifier (10 mV, 1150 Hz). The morphology of the Au particles was deduced from filled state images (negative sample bias) for which the impact of the electronic structure on the imaging contrast was smallest.

III. RESULTS AND DISCUSSION

A. Morphological characterization of the Au deposits

STM topographic images of 20-, 30-, and 40-ML-thick CaO films covered with 0.7-ML Au are displayed in Fig. 1. Both, particle density and shape were found to vary considerably with the oxide thickness. In the thin-film regime (<25 ML), exclusively flat Au islands are observed that homogenously cover the oxide surface with a mean density of $\sim 15 \times 10^{11}$ cm^{-2} [Fig. 1(a)]. Similar 2D islands are found also inside the holes that still expose the Ca-Mo-O wetting layer. Closer inspection reveals that most of the islands comprise a single Au layer only with some of them having a small second-layer patch on top. The monolayer height together with a typical island diameter of 4–6 nm yield a mean aspect ratio (height to diameter) of 0.07 for Au deposits in the low-thickness regime [Fig. 2(a)]. The islands typically have a distorted hexagonal shape, indicating the development of (111)-oriented Au sheets on the CaO surface [Fig. 3(a)]. This growth orientation is compatible with the low surface-free energy of this particular gold plane and has been revealed for Au islands on MgO(001) films before.[24] At small negative bias, a characteristic stripe pattern appears on top of the islands, being characterized by a line spacing of (7 ± 1) Å [Figs. 3(b) and 3(c)]. Two orthogonal patterns are found in which the bright lines run along the two equivalent CaO[100] directions. It is assigned to a (3×1) moiré structure formed between the CaO square lattice and the hexagonal atom arrangement of gold [Fig. 3(d)]. In this configuration, every fifth [211]-oriented Au row sits on top of a [100]-oriented Ca row, a registry that requires 4% compression of the gold lattice [Fig. 3(d)]. We suspect that those Au atoms have a larger interface distance due to the repulsive Au-Ca interactions and, consequently, appear brighter in the STM images.[25] The remaining Au atoms are able to occupy more favorable O-top and bridge sites, resulting in a shorter binding length and a reduced topographic contrast.[26] We note that any electronic contribution to the STM contrast is neglected at this point for the sake of simplicity. Our moiré-type structure model correctly predicts the spacing and orientation of the Au line pattern and is consistent with the fact that the line's direction

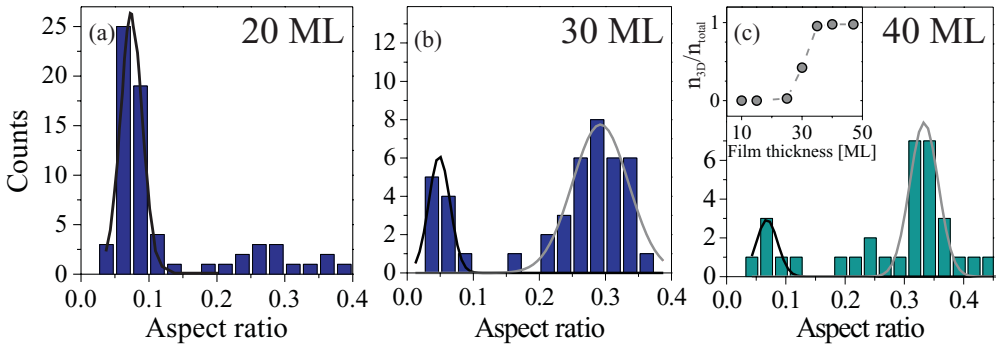

FIG. 2. (Color online) Histograms of Au-particle shapes, defined by the height-to-diameter ratio, for differently thick CaO films. STM images used for this analysis have been taken at negative sample bias (− 4 to − 6 V) in order to minimize electronic effects on the morphology. The histograms in (b) and (c) display a bimodal shape distribution due to the coexistence of 2D and 3D deposits. The inset in (c) shows the relative abundance of 2D versus 3D particles as a function of film thickness.

deviates by ∼30° from the Au-island edges. Information on the electronic structure of the Au islands can be found in Sec. C of this paper.

When increasing the CaO thickness above 25 ML, a change in the Au-particle morphology is observed [Fig. 1(b)]. Although the monolayer islands still are detectable as faint depressions in the surface, they now coexist with 3D deposits that display an enhanced aspect ratio of (0.3 ± 0.1). Surprisingly, almost no intermediate particle geometries are found in the STM images, and the corresponding shape histogram shows a pronounced bimodal distribution for the 2D and 3D deposits [Fig. 2(b)]. Moreover, particles of different geometry prefer different nucleation positions on the CaO film. Whereas, the flat islands are found on the plain oxide terraces, the 3D particles exclusively appear on the CaO dislocation network. Apparently, defects are required to form 3D deposits, whereas, monolayer islands are stabilized only on the ideal terraces. Further thickening of the oxide film causes the number of 3D particles to increase with respect to their 2D counterparts [Fig. 1(c)]. Whereas, nearly half the islands are of monolayer type at 30-ML thickness, this number reduces to 10% and 5% for 35- and 40-ML thick films, respectively. Above this critical thickness, hardly any 2D islands are detected in the STM images anymore [Fig. 2(c), inset]. As mentioned before, the aspect ratio of individual particles does not reflect this global evolution, and the deposits belong either to the 2D or the 3D category. Consequently, the bimodal shape distribution also is preserved on 40-ML-thick CaO films, and only the relative heights of the two maxima change [Fig. 2(c)]. We note that the crossover in particle dimensionality is accompanied by a change in their areal densities from 15×10^{11} at 20 ML to 7.5×10^{11} and 6.0×10^{11} cm^{-2} at 30- and 40-ML films, respectively.

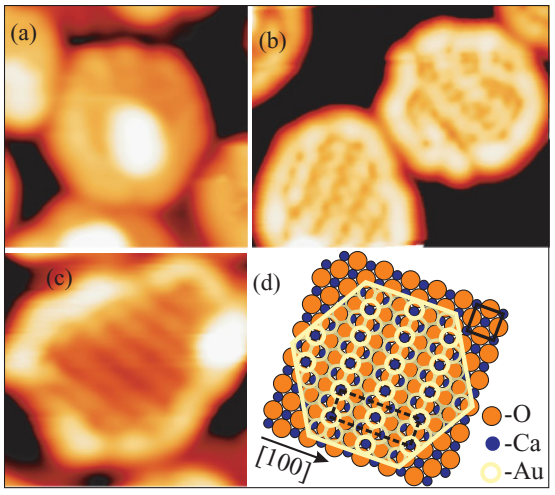

FIG. 3. (Color online) STM topographic images of monolayer Au islands on a 20-ML-thick CaO film. (a) Hexagonal island with a tiny second-layer patch on top (6×6 nm^2). (b) and (c) Monolayer islands with characteristic line patterns (8×6 and 6×6 nm^2). The pattern is assigned to a moiré structure formed between the hexagonal Au and the square CaO lattice. The respective structure model is shown in (d).

B. Discussion of the Au-particle morphology

The main finding of our growth analysis is a transition from 2D to 3D particle morphologies that occurs between 25- and 35-ML thickness of the CaO film [Fig. 2(c)]. The 3D growth regime observed beyond this value corresponds to the Volmer-Weber mode that is characteristic for metals on inert oxide surfaces and is governed by the small interface adhesion.[9,12,13] On ultrathin oxide films on metal supports, a 2D growth mode might prevail being induced by charge-transfer processes from the metal into the adparticles.[16,18] The electron exchange is enabled by the low work function of the thin-film system in conjunction with the high electron-affinity of gold. For the MgO/Mo(001) system, for example, the work-function decline has been ascribed to a cooperative effect between a suppressed Mo surface dipole and an interface dipole due to an electron flow from the oxide into the electronegative Mo.[27,28] Similar processes are expected to take place at the CaO/Mo interface as CaO is even more basic than the isostructural MgO and, hence, a better electron donor. The low work function causes the Fermi level of the Au deposits to shift below the one of the thin-film support, triggering an electron transfer into the gold. The electron-rich adislands now exhibit an enhanced interface adhesion, being mediated by electrostatic and polaronic interactions with the oxide lattice. To maximize

this effect, the gold spreads into 2D sheets on the CaO surface and returns to the common 3D mode only if the electron transport is inhibited at large oxide thicknesses.

At first glance, our experimental observations seem to be in-line with this established growth model; however, there is a distinct deviation from earlier studies.[18,24] Whereas, the 2D/3D growth transition occurs at 5–8-ML thickness on MgO/Ag(001), it is shifted to 25–35 ML on CaO/Mo(001), a value that is much larger than typical electron-tunneling lengths in insulating materials. We assign this marked difference to the specific nature of the CaO/Mo interface as already sketched in Sec. II. In the initial growth stage, Ca and Mo form a mixed oxide with 25% of the cationic sites being occupied by Mo in order to improve the lattice match with the Mo(001) surface.[22] However, the Mo impurities are relevant not only from a structural view point, but also actively modify the electronic properties of the mixed oxide. As shown in recent density-functional theory calculations, Mo is susceptible to become oxidized in the CaO lattice, i.e., it increases its charge state from $+2$ to $+3$.[20] The released electron that had initially occupied a Mo d level inside the band gap either enters the metal substrate or gets transferred into suitable adspecies. Whereas, the first route affects the Au growth behavior only indirectly by further reducing the CaO work function, the second one produces anionic gold directly. Charge-transfer processes mediated by Mo impurities in the CaO lattice, thus, might explain the larger critical thickness for the 2D/3D crossover in the Au growth. We suspect that the Mo donors not only are inserted into the interface layers where formation of a mixed oxide can be proven directly with Auger spectroscopy, but also affect the subsequent planes yet without developing a structurally well-defined phase. Still, the Mo content seems sufficient to stimulate electron transfer into the Au adspecies and to promote their 2D growth. We note that formation of 2D Au islands has been observed even on CaO films of more than 60-ML thickness when the Mo was incorporated intentionally into the oxide matrix.[20] In this case, the external dopants take over the role of the interdiffused Mo species at the interface, extending the 2D growth mode to arbitrary thicknesses.

Interestingly, as long as the 2D Au islands appear on the CaO surface, they adopt rather similar sizes and aspect ratios. Even close to the crossover thickness, when the number of Mo donors already has decreased substantially, the islands keep their 2D geometry and contain no more than 500 atoms. This unique behavior that also leads to the bimodal particle-shape distribution in Fig. 2(c) suggests a self-limiting growth of Au on the flat CaO terraces. Evidently, atoms do neither attach to the perimeter nor climb on top of the 2D islands once the final size has been reached. We take this observation as further evidence for the charged nature of the Au deposits. Every adatom that integrates into the 2D system increases its total charge and, hence, the impact of internal electron-electron repulsion. Moreover, the extra electrons that localize mainly at the island perimeter[29] build up an electrostatic barrier for the following atoms that are negatively charged as well. Both effects will terminate the island growth at a critical size. For Au islands on MgO thin films, the stopping condition has been identified as the point when each boundary atom has taken up one full electron, although atoms in the interior might still be close to neutral.[29] Interestingly, no self-terminated growth is revealed for particles at the CaO dislocation lines where 3D deposits, comprising several thousands of atoms, are found. A possible reason for this difference is the availability of electron traps along the oxide line defects, which are able to drain the extra electrons from the deposits and to remove the growth obstacle.

C. Electronic properties of monolayer Au islands on thin CaO films

The following section addresses the electronic structure of supported Au particles as measured with STM conductance spectroscopy. We concentrate on monolayer islands that may display unusual properties due to their reduced dimensionality and charged nature.

1. Field-emission spectra

We first discuss spectra taken at bias voltages around the work function of the system as shown in Fig. 4(a) for a bare and an Au-covered CaO film of 20-ML thickness. The spectra are characterized by a series of dI/dV maxima with the first peak occurring at 3.5 V for the bare film but at 4.5–4.7 V for the Au islands. Electron transport in this bias range is governed by the field-emission resonances (FERs), which can be considered as image potential states above the surface that are fixed in energy by the sample work function and the tip-electric field. [30] The different positions of the FERs above the adislands and the bare film become evident also in the pronounced contrast changes in the high-bias STM images [Fig. 4(b)]. Whereas, below 3.0 V, the Au islands appear as flat protrusions in correspondence with their monolayer height, a contrast reversal takes place at higher biases. Beyond the first CaO-FER at 3.5 V, the Au islands adopt the same contrast as the surrounding oxide regions, and only some small second-layer Au patches remain visible [see solid ovals in Fig. 4(b)]. At

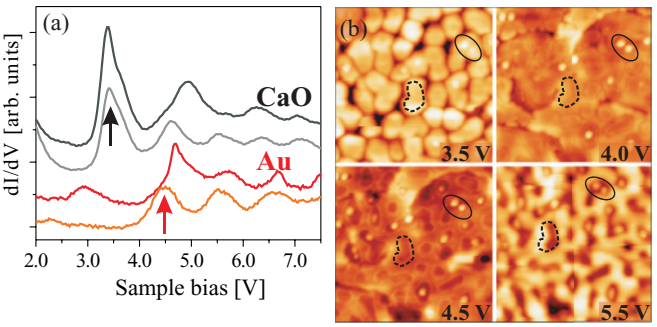

FIG. 4. (Color online) (a) STM conductance spectra taken with enabled feedback loop on 20-ML CaO with and without Au islands. A series of field-emission resonances becomes visible with the lowest ones being marked by arrows. (b) Corresponding STM images taken in the same bias window (40×40 nm^2). Due to different contributions of the field-emission resonances to the electron transport, the monolayer Au islands undergo a contrast reversal as a function of bias voltage. The dashed and solid lines are guides to the eye and mark identical islands in each panel.

even higher biases, the adislands gradually turn into faint depressions and finally appear as holes inside the bright oxide surface. Only the island perimeter is excluded from this evolution and shows up with bright contrast throughout the bias series. The observed contrast reversal mimics the contribution of the FERs to the electron transport between tip and sample. Below the first FER, the apparent height is governed by the true elevation and the available state density of certain surface sections. Both contributions determine the bright appearance of Au islands on the CaO surface. The situation changes once the first CaO-FER is reached, and an effective electron-transport channel becomes accessible into the oxide film. As no comparable channel exists on the Au islands, their apparent height declines with respect to the CaO and finally turns negative. The contrast remains reversed even after crossing the first Au-FER at ~4.5 V because the second CaO resonance state already is reached at this condition. We note that no bias-dependent contrast inversion takes place at negative polarity, and we, therefore, used negative-bias images to deduce reliable morphological information on the CaO-supported Au islands.

The deviating positions of the FERs on bare and Au-covered CaO films are explained with different local work functions that provide different offsets to the FER energies.[31] The up-shift in the gold spectra translates into a higher work function of the islands with respect to the adjacent CaO surface. As discussed before, the CaO film lowers the Mo(001) work function ($\phi = 4.53$ eV) by at least 1.0 eV due to the positive dipole formed at the metal-oxide interface.[27] Bulk gold, on the other hand, has a higher ϕ value (5.25 eV) in agreement with the observed trend in the FER spectra. However, the shift in the FERs cannot be explained entirely with a high gold work function because the islands are too small to reach the bulk limit of ϕ. We, therefore, suspect that the anionic nature of the aggregates influences the FER energies, as well. Electron accumulation in the adislands, combined with a positive charging of the Mo donors beneath, gives rise to an electrostatic dipole that points away from the surface and raises the local work function. In contrast, an electron flow out of the admetal would lower the work function, which is incompatible with the experimental results. At this point, we are unable to disentangle both effects as neither the surface dipole formed between $Au^{\delta-}$ and $Mo^{\delta+}$ nor the work function of neutral Au islands is known.

We note, in passing, that a similar conclusion on the Au charge state can be drawn from the CaO conduction-band (CB) onset, measured before and after Au exposure with conductance spectroscopy. Whereas, on pristine 20-ML thick films, the onset position is reached at 1.6 V, it shifts to 1.8 V after dosing [Fig. 5(a)]. The band shift that affects the valance band in a similar way reflects the response of the dielectric film to the surface dipole created between the anionic Au islands and the $Mo^{\delta+}$ centers in the film [Fig. 5(b)].[32,33] The excess charges inside the adislands destabilize the electronic states in the CaO planes beneath and trigger their shift to higher energies. Both results, the up-shift of the FERs and the CaO bands, therefore, support the main conclusions of our growth discussion, namely, that of a charge transfer from the CaO film into the Au islands.

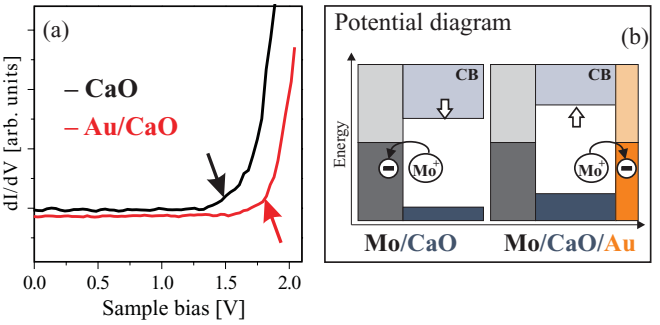

FIG. 5. (Color online) (a) STM conductance spectra taken in the region of the CaO CB onset with and without Au particles. The up-shifted CB band in the presence of the adislands indicates the negative charge state of gold on the CaO films. The mechanism is sketched in the potential diagram shown in (b). Whereas, the positive dipole at the Mo-CaO interface leads to a down-shift of the CaO bands, the negative dipole induced by the Au islands opposes this trend.

2. Low-bias spectra

Insight into the intrinsic electronic structure of the Au islands is obtained from conductance spectra taken around the Fermi level (E_F). We note that this spectroscopy mode only is possible for thin CaO films (<20 ML) that exhibit enough low-bias conductivity. A set of dI/dV spectra, taken on the monolayer Au islands labeled in the inset, is shown in Fig. 6. The main features of all curves are sharp and nearly equidistant dI/dV maxima that occur symmetrically on both sides of E_F. For a typical Au island of ~5-nm diameter, the peak-peak distance varies between 80 and 120 mV, although not every maximum is equally well developed (Spectrum 1). In contrast, a two-times larger peak spacing is revealed for islands with an emerging second layer (Spectrum 2). In general, the detected

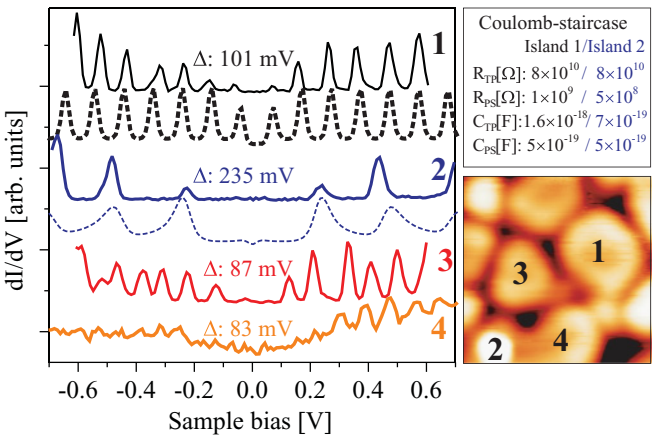

FIG. 6. (Color online) STM conductance spectra taken on four Au islands grown on a 20-ML-thick CaO film. The probed islands are shown in the inset (12×12 nm^2). All spectra exhibit a series of equidistant peaks characterized by a mean-energy spacing Δ. Each peak can be correlated with a Coulomb-charging event in which the electron count on the island changes by 1. The upper two spectra were fitted with an analytical model that describes the double-barrier STM junction as a series of resistor/capacitor pairs.[35] The fit parameters are given in the inset on the upper right (see text for details).

peak separations depend on the set point for spectroscopy, and a larger bias, hence, a wider tip-sample gap, causes the maxima to move away from each other. The regular peak structure observed here is identified readily as a Coulomb staircase, being induced by the double-barrier nature of our tip-sample junction.[34,35] The Au islands can be considered as floating electrodes, being electrically isolated from the tip and sample by the vacuum barrier and the insulating CaO film, respectively. Electron transport through the junction, thus, involves transient charging of the adisland for which the Coulomb repulsion between the incoming electron and the charges on the island needs to be overcome. The first electron from an outer electrode reaches the Au island if its energy exceeds the Coulomb barrier, a condition that gives rise to the first dI/dV peak. The following maxima mark subsequent charging events, each of them increasing (decreasing) the electron count on the Au islands by 1 at positive (negative) sample bias.

To characterize the tunneling barriers above and below the Au islands, we have fitted the experimental data with an analytical approach developed by Hanna and Tinkham.[36] There, the double-barrier junction is modeled with an equivalent circuit diagram composed of two resistor-capacitor pairs connected in series. Whereas, the first pair (R_{TP},C_{TP}) describes the electron flow from the tip to the particle, i.e., across the vacuum barrier, the second one mimics the effect of the oxide film (R_{PS},C_{PS}). The model indeed reproduces the experimental data when using the preset junction resistance of 80 GΩ and optimizing the two capacitors accordingly. The capacitance of the 20-ML CaO film C_{PS} has been fitted with 5×10^{-19} F. This value is in reasonable agreement with a simple plate-capacitor description of the Au-CaO-Mo sandwich structure $C = \varepsilon_0 \varepsilon_r \frac{A}{d}$, which yields a capacitance of 3.7×10^{-19} F for an island size A of 20 nm^2, a film thickness d of 4.8 nm, and a CaO dielectric constant of $\varepsilon_r = 10$. The tip-particle capacitance C_{TP}, on the other hand, exhibits much larger variations and is, in fact, responsible for the spread in the detected peak separations. For monolayer Au islands, C_{TP} is roughly three times larger than C_{PS}, reflecting the smaller tip-particle versus particle-support distances. The presence of a second layer on top of the Au islands substantially reduces C_{TP} as the active area on the particle side of the capacitor becomes smaller. It is this decrease in the tip-particle capacitance that is responsible for larger Coulomb charging energies, hence, larger spacing of the dI/dV peaks in Au bilayer spectra (Fig. 6, Spectrum 1 versus Spectrum 2). We note that an accurate fitting of the Coulomb staircase always requires a small fractional charge on the Au islands that amounts to $0.5|e|$ in Spectrum 2, for example.[36] Unfortunately, no information on the absolute charges on the island can be deduced from this number as the Coulomb staircase remains unchanged when adding/removing a full electron.

Whereas, Au islands on the CaO films are well suited to study Coulomb-charging effects due to a planar geometry, an analysis of their electronic properties is difficult as the very same charging peaks interfere with tiny dI/dV modulations induced by confinement effects in the nanoislands. Insight into the Au electronic structure might still be obtained from dI/dV maps taken at positive bias, although the accessible bias range is limited again by the diminishing conductance

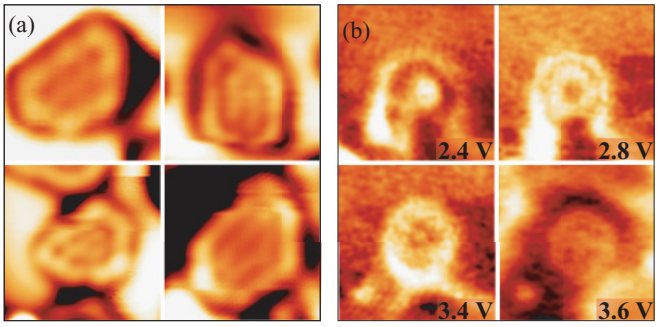

FIG. 7. (Color online) (a) STM conductance maps of four Au islands on a 20-ML-thick CaO film taken at a 2.0-V sample bias (7×7 nm^2). The line patterns inside the islands are assigned to charge-density waves induced by electron confinement. (b) Conductance series displaying the evolution of the standing-wave pattern with sample bias (7×7 nm^2). Such maps can only be acquired in a limited bias range, given by the vanishing film conductivity and the onset of the field-emission resonances at low and high biases, respectively.

of the CaO films below 2.0 V. The respective maps display a characteristic line pattern on top of the islands that varies with bias voltage. Whereas, on large islands, the pattern comprises a bright perimeter plus several parallel lines in their interiors [Fig. 7(a)], a number of concentric rings is observed on smaller roundish patches. At least four of those patterns are resolved in Fig. 7(b) until the contrast vanishes at high bias. The first one at 2.5 V is characterized by a bright maximum in the island center and a protruding ring at the perimeter. With higher bias, the inner ring moves outward, and new maxima appear in the center of the islands.

We assign those line patterns to charge-density waves induced by discrete eigenstates in the spatially confined electronic systems.[37–39] As the experimental data only represent a small cutout of the complete electronic structure, we only discuss the nature of these quantum states on a qualitative level. The states are incompatible with Au 6s orbitals at the Γ point, which should be occupied and located below E_F, whereas, states with dominant 6p character are better candidates.[29,39] Confining such free-electron-type states in a hexagonal potential produces charge-density patterns that exhibit a central maximum/minimum surrounded by several concentric rings.[37,40,41] In elongated islands, the hexagonal symmetry is broken, and the rings transform into short straight lines as revealed in our dI/dV maps (Fig. 7). Given the obvious experimental limitations, we refrain from a more detailed analysis and just state that the observed standing-wave patterns indicate electron quantization effects in the Au nanoislands.

The final issue of this paper concerns the fact that the perimeter of larger Au islands appears bright independent of the selected bias voltage [Figs. 4(b) and 7(a)]. At first glance, this seems to be incompatible with the quantization picture where charge-density patterns with little edge intensity should exist as well. However, earlier papers on MgO-supported Au islands revealed that a bright perimeter is characteristic for charged islands as it reflects the localization of excess electrons in specific edge states along the perimeter.[29] Tunneling into those states produces the bright brim around the islands that

also is evident in our images. We take this finding as additional evidence for the charged nature of monolayer Au islands on the CaO films.

IV. CONCLUSIONS

STM experiments on CaO/Mo(001) films revealed a crossover from 2D to 3D gold particle shapes with increasing film thickness, being indicative of a charge-mediated growth behavior on the thin-film support. Whereas, gold becomes anionic and spreads into monolayer islands below 25-ML thickness, it remains neutral and grows into compact 3D deposits on thicker films. This result is in line with earlier Au growth papers on MgO and alumina films[18,21] and reflects the universal character of charge-driven metal-oxide interactions in the thin-film limit. However, the critical film thickness for the dimensionality crossover was found to be five times larger for CaO compared to similar systems. The difference is explained by the presence of Mo impurities that diffuse from the Mo support into the oxide film during preparation. Due to their multivalent nature, the Mo ions are able to transfer electrons into the Au adisland and act as intrinsic charge donors. Given the limited diffusion length of Mo inside the CaO lattice, the Mo concentration diminishes with film thickness, reestablishing the common 3D growth regime of Au on a 25- to 35-ML-thick film. However, the charge-mediated growth regime can be stabilized for any thickness if the Mo impurities are introduced via external doping.[20]

The availability of well-shaped Au particles on rather thick oxide films opens interesting possibilities for investigating the interplay between geometry, electronic, optical, and chemical properties of supported metal deposits. As sketched in this paper, the 2D Au islands are subject to pronounced quantization effects, which might be accompanied by interesting optical aspects. Moreover, the monolayer Au sheets might feature deviating chemical properties with respect to their 3D counterparts as they exhibit a large number of perimeter atoms that enable simultaneous interactions of adsorbates with the metal and the oxide support. The high density of excess electrons at the island perimeter, being the actual reason for the 2D growth, is expected to alter this reactivity pattern even more drastically. Experiments on the chemical nature of the 2D Au islands are envisioned in the future as they might provide insight into the interplay between particle morphology and chemical properties that is in the center of catalysis research.

ACKNOWLEDGMENTS

We are grateful for financial support from the DFG Excellence-Initiative "Unicat" and for theoretical insights into the nature of the Mo dopants as provided by G. Pacchioni and L. Giordano.

*nilius@fhi-berlin.mpg.de

[1] *Clusters of Atoms and Molecules*, edited by H. Haberland (Springer, Berlin, 1994); *Metal Clusters*, edited by W. Ekardt (Wiley, Chichester, 1999).
[2] P. Gruene, D. M. Rayner, B. Redlich, A. F. G. van der Meer, J. T. Lyon, G. Meijer, and A. Fielicke, Science **321**, 674 (2008).
[3] U. Kreibig and M. Vollmer, *Optical Properties of Metal Clusters* (Springer, Berlin, 1995).
[4] T. Wenzel, J. Bosbach, F. Stietz, and F. Trager, Surf. Sci. **432**, 257 (1999).
[5] J. Hoffmann, S. Schauermann, J. Hartmann, V. P. Zhdanov, B. Kasemo, J. Libuda, and H.-J. Freund, Chem. Phys. Lett. **354**, 403 (2002).
[6] S. Mostafa, F. Behafarid, J. R. Croy, L. K. Ono, L. Li, J. C. Yang, A. I. Frenkel, and B. Roldan Cuenya, J. Am. Chem. Soc. **132**, 15714 (2010).
[7] M. P. Pileni, J. Phys. Chem. C **111**, 9019 (2007).
[8] M. Pelton, J. Aizpurua, and G. Bryant, Laser Photonics Rev. **2**, 136 (2008).
[9] E. Bauer and J. H. van der Merwe, Phys. Rev. B **33**, 3657 (1986).
[10] G. Wulff, Z. Kristallogr. **34**, 449 (1901).
[11] D. Chatain, J. Rivolleti, and N. Eustathopoulos, J. Chem. Phys. B **83**, 561 (1986); D. Chatain and J. J. Metois, Surf. Sci. **291**, 1 (1993).
[12] C. T. Campbell, Surf. Sci. Rep. **27**, 1 (1997).
[13] M. Bäumer and H.-J. Freund, Prog. Surf. Sci. **61**, 127 (1999).
[14] H.-M. Benia, N. Nilius, and H.-J. Freund, Surf. Sci. Lett. **600**, L128 (2006).
[15] M. A. Brown, Y. Fujimori, F. Ringleb, X. Shao, F. Stavale, N. Nilius, M. Sterrer, and H.-J. Freund, J. Am. Chem. Soc. **133**, 10668 (2011).
[16] D. Ricci, A. Bongiorno, G. Pacchioni, and U. Landman, Phys. Rev. Lett. **97**, 036106 (2006).
[17] G. Pacchioni, L. Giordano, and M. Baistrocchi, Phys. Rev. Lett. **94**, 226104 (2005).
[18] M. Sterrer, T. Risse, M. Heyde, H.-P. Rust, and H.-J. Freund, Phys. Rev. Lett. **98**, 206103 (2007).
[19] N. Mammen, S. Narasimhan, and S. de Gironcoli, J. Am. Chem. Soc. **133**, 2801 (2011).
[20] X. Shao, S. Prada, L. Giordano, G. Pacchioni, N. Nilius, and H.-J. Freund, Angew. Chem., Int. Ed. **50**, 11525 (2011).
[21] N. Nilius, M. V. Ganduglia-Pirovano, V. Brázdová, M. Kulawik, J. Sauer, and H.-J. Freund, Phys. Rev. Lett. **100**, 096802 (2008).
[22] X. Shao, N. Nilius, P. Myrach, H.-J. Freund, U. Martinez, S. Prada, L. Giordano, and G. Pacchioni, Phys. Rev. B **83**, 245407 (2011); X. Shao, P. Myrach, N. Nilius, and H.-J. Freund, J. Phys. Chem. C **115**, 8784 (2011).
[23] J. Wollschläger, D. Erdos, H. Goldbach, R. Hopken, and K. M. Schröder, Thin Solid Films **400**, 1 (2001).
[24] S. Benedetti, P. Myrach, A. di Bona, S. Valeri, N. Nilius, and H.-J. Freund, Phys. Rev. B **83**, 125423 (2011).
[25] J. Goniakowski and C. Noguera, Interface Sci. **12**, 93 (2004).
[26] A. Del Vitto, G. Pacchioni, F. O. Delbecq, and P. Sautet, J. Phys. Chem. B **109**, 8040 (2005); S. Sicolo, L. Giordano, and G. Pacchioni, J. Phys. Chem. C **113**, 16694 (2009).
[27] L. Giordano, F. Cinquini, and G. Pacchioni, Phys. Rev. B **73**, 045414 (2006).
[28] J. Goniakowski, and C. Noguera, Phys. Rev. B **79**, 155433 (2009).
[29] X. Lin, N. Nilius, M. Sterrer, P. Koskinen, H. Häkkinen, and H.-J. Freund, Phys. Rev. B **81**, 153406 (2010).

[30]G. Binnig, K. H. Frank, H. Fuchs, N. Garcia, B. Reihl, H. Rohrer, F. Salvan, and A. R. Williams, Phys. Rev. Lett. **55**, 991 (1985).
[31]O. Y. Kolesnychenko, Y. A. Kolesnichenko, O. I. Shklyarevskii, and H. van Kempen, Physica B **291**, 246 (2000).
[32]D. A. Bonnell, Prog. Surf. Sci. **57**, 187 (1998).
[33]U. Martinez, J.-F. Jerratsch, N. Nilius, L. Giordano, G. Pacchioni, and H.-J. Freund, Phys. Rev. Lett. **103**, 056801 (2009).
[34]K. Sattler, Z. Phys. D: At., Mol. Clusters **19**, 287 (1991); M. Amman, R. Wilkes, E. Ben-Jacob, P. D. Maker, and R. C. Jaklevic, Phys. Rev. B **43**, 1146N (1991).
[35]N. Nilius, M. Kulawik, H.-P. Rust, and H.-J. Freund, Surf. Sci. **572**, 347 (2004).
[36]A. E. Hanna and M. Tinkham, Phys. Rev. B **44**, 5919 (1991).
[37]I. Barke and H. Hovel, Phys. Rev. Lett. **90**, 166801 (2003).
[38]N. Nilius, T. M. Wallis, and W. Ho, Science **297**, 1853 (2002); J. Lagoute, X. Liu, and S. Fölsch, Phys. Rev. Lett. **95**, 136801 (2005).
[39]X. Lin, N. Nilius, H.-J. Freund, M. Walter, P. Frondelius, H. Honkola, and H. Häkkinen, Phys. Rev. Lett. **102**, 206801 (2009).
[40]J. Li, W.-D. Schneider, S. Crampin, and R. Berndt, Surf. Sci. **422**, 95 (1999).
[41]K. Schouteden, E. Lijnen, D. A. Muzychenko, A. Ceulemans, L. F. Chibotaru, P. Lievens, and C. van Haesendonck, Nanotechnology **20**, 395401 (2009).